J Mater Sci (2008) 43:4953–4961
DOI 10.1007/s10853-008-2729-4

Young's modulus of low-pressure cold sprayed composites: an analysis based on a minimum contact area model

Mark Lubrick · R. Gr. Maev · F. Severin · V. Leshchynsky

Received: 13 July 2007 / Accepted: 16 May 2008 / Published online: 3 June 2008
© Springer Science+Business Media, LLC 2008

Abstract A theoretical and mathematical model based on minimum contact area (MCA) is developed to explain the bonding that takes place in the low-pressure gas dynamic spray (LPGDS) process. It is shown that by normalizing this MCA it is possible to compare the relative elastic modulus as a function of porosity. Theoretical predictions of relative elastic modulus are compared against results obtained through acoustic analysis and it is found that the correlation between is dependent on the porosity. For low porosity, the experimental and theoretical results differ substantially, while for higher porosity there seems to be good agreement between the two. To explain this behaviour it is theorized that full adiabatic shear bands (ASB) are created between only some of the particles. The higher porosity causes higher strain in the samples and thus more local deformation of the particles. This, in turn, causes more actual ASB formation. Since the theoretical model assumes full ASB formation, only the higher porosities cause enough strain to have a comparable relative elastic modulus. For the lower porosities, the local strain is less, and some of the bonds will not achieve full ASB formation. For these cases, the relative elastic modulus will be lower than that predicted.

Introduction

The cold or gas dynamic spray (GDS) process is a type of thermal spray technique that relies on the high velocity of particles rather than on high heat. The severe plastic deformation of particles during GDS processes results in both the consolidation and strengthening of the resultant coating. This suggests that the extensive plastic flow of a particulate material is the main process that governs the structural formation of the coating. The metals are well-known materials, which in many cases exhibit excellent ductility and low flow stress. Metal particles with high kinetic energy build up a dense coating due to deformation upon impact [1]. Thus, the macroscopic mechanical properties of composites are strongly conditioned by the bulk properties of the constituents; they are also influenced by the mechanical behaviour of the matrix/reinforcement interfaces.

A detailed analysis of the bonding process has been undertaken by Borchers et al. [2, 3]. As shown in this study of the interfaces in high-pressure GDS process, inter-particle bonding areas do not form a complete bonding network. In fact, some of the bonding areas exhibit microstructural features such as jets.

Using transmission electron microscopy (TEM), several remarkable features are noted at the interface [2, 3]. In some locations within Al, there appears a tangled structure, where the interface has bifurcations; here, a thin stripe of material with a thickness of some nanometers seems to be interlaced. The Al particles interface is, in fact, somewhat wavy on the order of some 100 nm, with the grains having low dislocation density. The grain size near the interface is about 500 nm. Copper coating GDS also exhibits a non-equilibrium grain boundary, which is characterized by ultrahigh dislocation densities adjacent to the grain boundaries. The microstructural features of Ni GDS coatings are similar to those of Cu. The particle–particle interfaces consist of nanosized grains and large grains with coffee-bean-like contrast, which is typical for shock-consolidated structures [4].

The above-described results clearly show that effective inter-particle bonding takes place only in local areas.

M. Lubrick (✉) · R. Gr. Maev · F. Severin · V. Leshchynsky
University of Windsor, Windsor, ON, Canada
e-mail: lubrick@uwindsor.ca

Moreover, the structure of the bonded areas is not uniform, influencing the interfacial mechanical properties as well. It seems reasonable to classify the inter-particle bonds as those made by (i) the melting of adjacent particles, (ii) adiabatic shear band formation with a phase transformation at the inter-particle contacts, and (iii) adhesion (Van-Der-Waals) forces.

At present time there are two primary issues of GDS that have not yet been completely defined: (i) the type of inter-particle bonds, and (ii) the surface area occupied by the definite type of inter-particle bonds that are created by the appropriate powder consolidation technique. The primary bonding structures (described above) may be characterized by definite macroscopic mechanical properties. Thus, based on the analysis of the mechanical properties, the structure of inter-particle bonds and the contact surface area data, it may in fact be possible to estimate the contribution of each bonding mechanism to the mechanical strength of the composite as a whole. Therefore, having characterized the inter-particle bonding mechanism, it seems it will be possible to determine the (i) macroscopic bonding strength, (ii) bonding surface area, and (iii) bonding area structure.

An in-depth analysis of the interfacial mechanical properties of GDS sprayed materials has not yet been performed from this perspective. The most detailed information characterizing the bonding of Al, Cu, Ni, and Ti may be found in a series of papers by Borchers et al. [2, 3] for HPGDS processes. These authors apply the Prummer [5] classification of bonding mechanisms in samples prepared by explosive compaction. The authors uncover three main bonding types:

(1) Adiabatic welding—the main bonding mechanism in the technique of explosive cladding. This bonding is characterized by adiabatic shear instability and jet formation at the welding interface. Prummer [5] calls this bonding "explosive welding", but since cold gas spraying is not a technique where explosive are used, we use the above expression in this work.
(2) Friction welding—here shear bands form which are not necessarily an adiabatic shear instability.
(3) Liquid phase sintering—the near-surface areas of the powder particles melt during compaction and subsequently weld together during cooling.

To find adiabatic welded interfaces, one has to look for jet formation as a result of adiabatic shear instabilities. Although it is not as easy to certify jet formation in low-pressure GDS (LPGDS) as it is in explosive welding, narrow bands of metallic materials observed between two particles could be evidence of jet occurrence (see Figs. 1 and 2). In addition, the plicate appearance of inter-particle region on the SEM micrograph (Fig. 3) may further suggest jet formation during LPGDS.

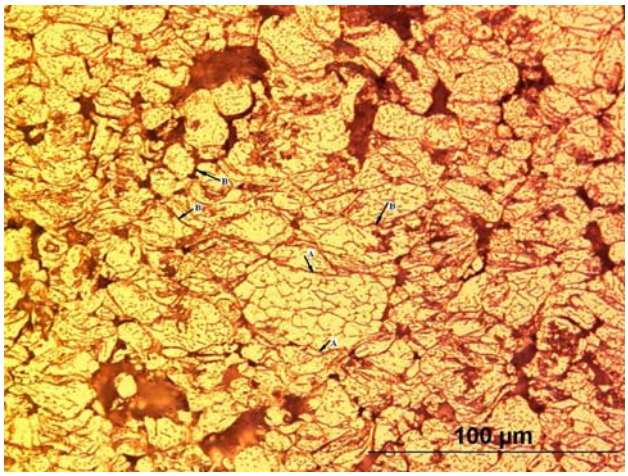

Fig. 1 Microstructure of aluminium low-pressure GDS coatings

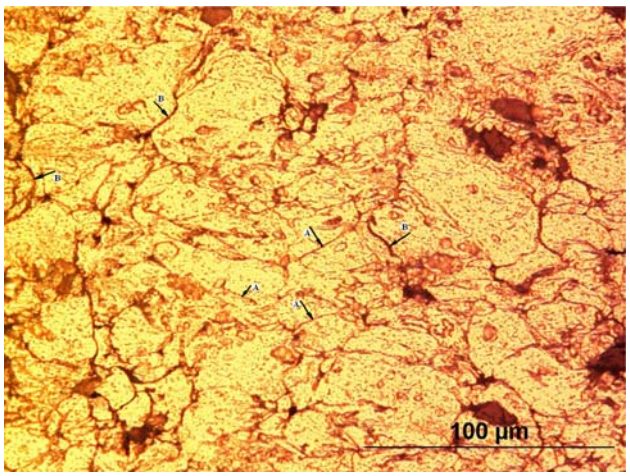

Fig. 2 Microstructure of aluminium and 10% alumina low-pressure GDS coatings

According to some [3], the microstructure of high-pressure GDS (HPGDS) copper coatings is characterized by a narrow zone of dynamically recrystallized material around the particle–particle interfaces. Further, they find no evidence for microstructural phenomena related to melting. Despite numerous studies [6], there is a decided lack of data concerning the microstructure characterization of composite coatings made by LPGDS. Of specific interest is the current lack of any studies on the elastic modulus of LPGDS.

Experimental procedure

Materials description

A large variety of metal matrix composites (MMCs) are employed, but by far the most widely studied materials are

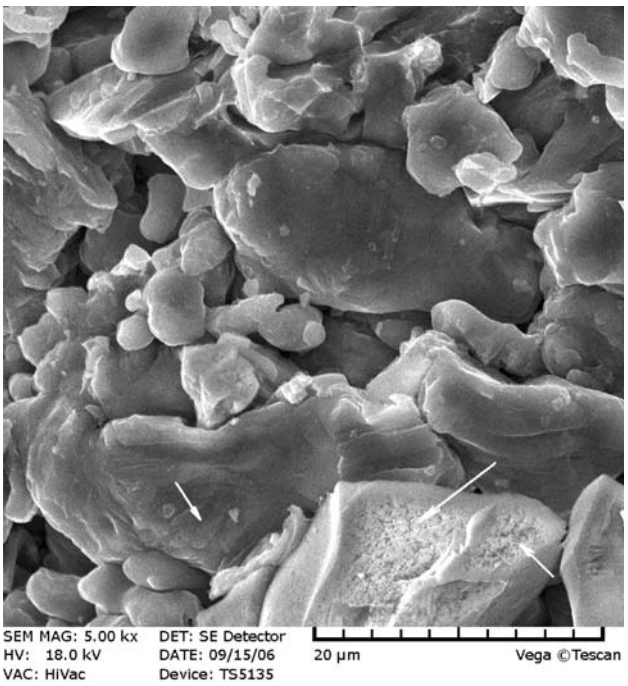

Fig. 3 SEM of aluminium and 10% alumina fracture surface

Al metal matrix composites. MMCs that are reinforced with ceramic particles offer high strength and a high elastic modulus, as well as favourable high-temperature properties as compared to the corresponding monolithic materials used as the matrix. The exact nature of the GDS technique used in the fabrication of MMCs has a significant effect on the overall properties of the product. Severe deformation of the particle interface due to shear instabilities must be achieved to obtain effective bonding between the matrix and the reinforcements.

Aluminium, copper, and nickel are the most common matrix elements employed in metal–ceramic composites; on the other hand, the most effective reinforcement particles are Al_2O_3, SiC, TiC, and others. For example, it has been reported [7] that the addition of TiC as a reinforcement improves the mechanical properties at both moderate and high temperatures. The composites chosen for this study are shown in Table 1.

It is widely recognised that the strength of the particle/matrix interface is of great importance with respect to the toughening of materials. In fact, the stiffness of the metal matrix is greatly increased by the presence of rigid particles. This has numerous additional advantages including an increase in both exploitation temperatures and thermal conductivity, as well as generating a larger coefficient of thermal expansion.

Preparation of samples

First, commercially available Al and Ni were blended homogeneously with reinforcement powders Al_2O_3 and TiC, respectively. By varying the average size and chemistry of the reinforcing ceramic phase (Table 1), diverse composite microstructures were obtained. Prior to spraying, the substrate surface was sandblasted using 300-mesh alumina grits. The substrates were then cleaned with acetone and methanol, dried in hot air and weighed before and after GDS. The composites were then sprayed using a portable apparatus equipped with an SST Centerline gun [8] to produce seven composites, which will be referred to hereafter as shown in Table 1. This system utilizes the injection of powder into the divergent part of a supersonic nozzle. The powder mixtures were supplied by a powder hopper and were injected into the supersonic portion of the nozzle near the throat area by means of a negative pressure developed by an accelerated stream of compressed air passing through the nozzle. The injected particles are accelerated in the high velocity air stream by the drag effect. To increase the air velocity and, ultimately the particle velocity, the compressed air can be preheated within a range from 100 °C to 700 °C. The pressure and temperature of the compressed air were monitored by a pressure gauge and a thermocouple positioned inside the gun. The gun was installed on an X–Y manipulator to scan the air-powder jet over the substrate surface. The

Table 1 Composite microstructure characteristics

Composite designation	Particle designation	Average particle size (µm)	Porosity (%)	Volume fraction of reinforcement (%)	Inter-particle distance (µm)
Al–Al_2O_3–1	Al_2O_3	10	3.1	10	187.5
Al–Al_2O_3–2	Al_2O_3	10	3.5	15	100.
Al–Al_2O_3–3	Al_2O_3	10	4.3	30	44.6
Al–Al_2O_3–4	Al_2O_3	45	4.9	50	10
Ni–TiC–1	TiC	20	7.5	10	90
Ni–TiC–2	TiC	20	8.1	20	57.1
Ni–TiC–3	TiC	20	9.5	30	33.3

compressed air pressure was kept constant at 0.5 MPa. The particle velocities at the exit plane of the supersonic nozzle, as measured by a Laser Doppler Velocimeter, were in the range of 550–650 m/s. The powder feeding rate was varied in the range of 0.5–1.5 g/s, while the standoff distance (measured from the exit of the nozzle to the substrate) was held constant at 10 mm. A rectangular nozzle with an exit aperture of 3.5 × 10 mm was used. Finally, the coatings were removed from the substrate for later analysis.

Determining the elastic modulus

Determining the value of the elastic modulus required two steps. First, a portion of each sample was used to determine density. Using a YDK01 (Sartorius) density determination kit and the Archimedean principle the density was determined to within an accuracy of 0.1%. The remaining portion of the samples was used to determine the longitudinal velocity of sound. The samples were ground and polished to give two parallel surfaces. The samples were then studied using an AM 1102 acoustical microscope (Tessonics) utilizing a 20 MHz flat transducer with a 3 mm diameter. Due to the porous nature of the material, it was undesirable to immerse the samples, and therefore Imagel R03-GEL1 (Tessonics) was used. The velocities were then determined by multiple trials (to prove accuracy) of the pulse echo overlap method.

Finally, using the experimentally determined values for velocity (v) and density (ρ), it was possible to determine the elastic modulus from:

$$E = \frac{v^2\rho(1+v)(1-2v)}{(1-v)}, \tag{1}$$

where v is Poisson's ratio, which we assumed was approximately 0.3 for all cases.

Effect of porosity on elastic constants: minimum contact area model

To increase the strength and stiffness of the composite materials, the reinforcement particle loading (ε_j) must be as high as possible. However, previous studies have shown that local reinforcement particle clustering might become a serious problem when the reinforcement loading is very high, e.g., at 30 vol.% [9]. Some ceramic reinforcement particles that may become clustered (e.g., SiC) usually cannot be sintered and bonded together at the consolidation temperature used for Al-based MMCs. Weak bonding between the ceramic particles may play a major role in microcrack initiation and growth, which can reduce the modulus of elasticity and fracture toughness of the MMCs. Therefore, high-volume fractions of reinforcement particles (>30 vol.%) are not usually used in current structural composites [9].

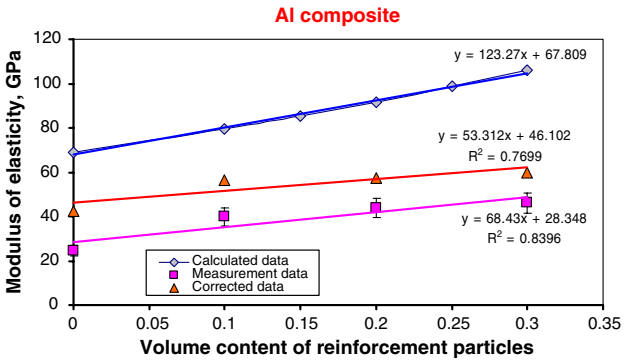

Fig. 4 Elastic Modulus of Al-based composites

The addition of high-modulus particles to a low-modulus metal matrix invariably leads to an increase in the modulus E of the composite over that of the matrix. As shown in Fig. 4, there is a strong dependence of the modulus composites upon ε_j, for Al-based composite reinforced with Al_2O_3 particles. This behaviour has been well documented [10, 11, 12]. Further, a variety of theories have been developed to explain the dependence of E upon ε_j. The one we considered was the Hashin–Shtrikman equation [13]:

$$E_c = \frac{E_m\left[E_m\left(1-\varepsilon_j\right)+E_r\left(\varepsilon_j+1\right)\right]}{E_r\left(1-\varepsilon_j\right)+E_m\left(\varepsilon_j+1\right)}, \tag{2}$$

where the subscripts m and r denote matrix and reinforcement, respectively.

In the case of GDS composite coatings, the porosity has great potential influence on the mechanical properties and, as such, must be taken into account. Porosity leads to a decrease in the elastic modulus because the load-bearing area of a material is reduced by the pores, with the stress becoming 'concentrated' near the pores [14]. For a body containing a low concentration of spherical pores, the MacKenzie [14] solution for the Young's modulus of the porous body is given by

$$E = E_0\left(1 - Af + Bf^2\right), \tag{3}$$

where E_0 is the Young's modulus of the dense material, f is the porosity fraction and A and B are constants of the order of 1.9 and 0.9, respectively.

The Young's modulus measurement results (Fig. 4) reveal the dependence $E = f(\varepsilon_j)$, for LPGDS Al-based composites is below those calculated with H–S model. The corrected data takes into account porosity according to Eq. 3 and results in an increase of E. It is important to note that the calculations of E with H–S Eq. 2 was based on the assumption that the structure of GDS composites is similar to infiltrated composites described by Kouzeli and Mortensen [10].

In the LPGDS case, the inter-particle bonding seems to be characterised by the adiabatic bonding in accordance with Borchers et al. [3]. The adiabatic bonding results in measured sound velocity similar to metallurgical bonding obtained in MMC casting or infiltrated MMC. However, the area of adiabatic bonds at the inter-particle contacts constitutes only a fraction of the total area of inter-particle contacts. This means that about 35–45% of the contact area does not have real adiabatic bonds, and thus leads to a decrease of Young's modulus. To more precisely characterise the formation of the inter-particle contacts, it is necessary to analyse, in detail, the actual Young's modulus—bonding area relations.

Development of MCA model for GDS process

The central feature of the GDS shock consolidation processes is that energy is dissipated by a shock wave as it traverses a powder medium. Inter-particle adiabatic shear band formation, vortices, voids, and particle fracture may occur due to plastic deformation. Meyers et al. [4] describe various energy dissipation processes that take place during shock consolidation: plastic deformation, inter-particle friction, microkinetic energy, and defect generation. If we assume sintering to be an ideal bonding process and characterize bonding by the relation v/v_o, we may compare our ultrasonic velocity measurement data with theoretical calculations of Mizusaki et al. [15] for sintering. In fact, Fig. 5 shows the sintering process according to a model based on the minimum contact area between particles [15]. In Fig. 5a, the particles are initially touching without any deformation. The model uses two sine functions to approximate the particle shape at all times. The first sine function represents the inter-particle distance (given as c). The second sine function represents the neck, or area of contact between subsequent particles. The neck is characterized by its diameter r_o and its thickness, $1-c$ (see Fig. 5). Figure 5b shows that as sintering takes place, the inter-particle distance will grow, as does the neck. The neck diameter will continue to widen until full density is reached, as in Fig. 5c where the diameter of the rod is given as $2a_t$. It is unnecessary however, to consider absolute values; in fact, a_t may be taken to equal ½ [15]. Figure 5c does show that when full density is achieved, r_o is equal to $2a_t$. Figure 5d shows the result of this interpretation using relative distances. The first sine function represents the particle from $0-c$, while the second function goes from $c-1$.

A "particle column" model of GDS shock consolidation is shown in Fig. 6. In this case, only particle deformation is responsible for the increase in neck diameter. The thickness of adiabatic shear bands for the GDS case is considered to

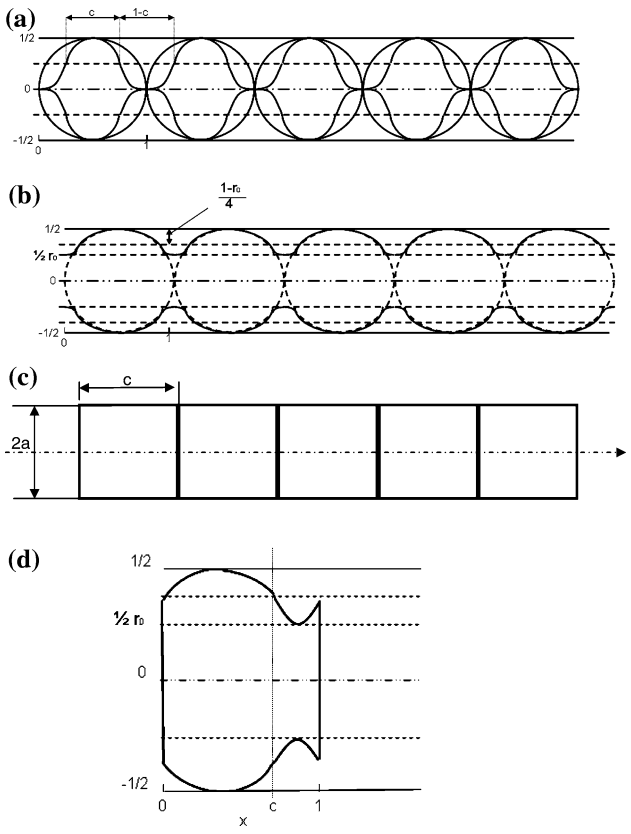

Fig. 5 (**a**) Mizusaki model-sine wave approximations, (**b**) during sintering, (**c**) fully sintered, (**d**) Relative value interpretation

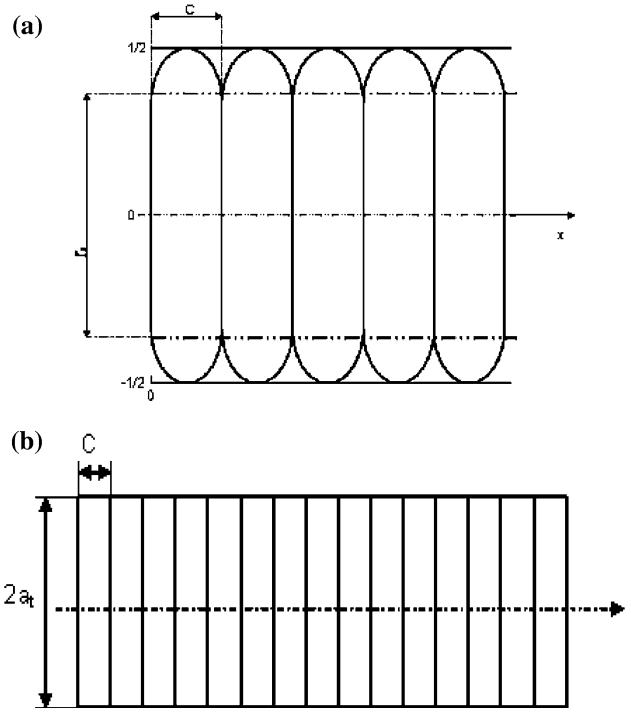

Fig. 6 (**a**) GDS model of densification, (**b**) at full density

be several microns [16]. For this reason, the thickness of the neck is approximated to be zero.

Another notable feature of the GDS shock consolidation model is that the particle deformation process is one in which the volume of the particle is unchanged. Thus, at any moment of deformation the solid material incompressibility equation $V_o = V_i$ is valid. When $a_t = a_o$, the relative density of the particle string (Fig. 5a) is the ratio V_o/V_{io}, where $V_{io} = \pi a_o^2 2a_o$.

The pore fraction may be calculated based on a particle string representative element (Fig. 5a):

$$\theta = \frac{V_{pore}}{V_{cyl}} = 1 - \frac{4a_o^3}{3a_t^2 c}, \tag{4}$$

where a_t is a radius of circumscribed cylinder. Taking into account $\frac{\rho}{\rho_o} = 1 - \theta$ the relative density is

$$\frac{\rho}{\rho_o} = \frac{(ma_t + nr_o)^2}{16a_t^2}, \tag{5}$$

where m and n are the coefficients of approximations that fit the following boundary conditions:

1. if $a_t = a_o$, $r_o = 0$ and $\rho/\rho_o = 0.33-0.6$ and
2. if $2a_t = r_o$, $\rho/\rho_o = 1$

Further adaptations have been made to this theory using results from the works of Mukhopadhyay and Phani [17, 18]. They approximated the normalized minimum contact area to be equal to the relative elastic modulus of the sample. The minimum contact area (MCA) is given by the smallest neck diameter. For the case of interest, this occurs when $F(x) = a_t r_0$, giving MCA = $(\pi/4)\, a_t^2 r_0^2$. The normalized minimum contact area (*NMCA*) is thus r_0^2. For all practical purposes, the *NMCA* is effectively equal to the relative modulus of elasticity E/E_0 [19]:

$$\text{NMCA} = r_0^2 \equiv \frac{E}{E_0}. \tag{6}$$

The GDS process results in real adiabatic bonds that are achieved within smaller contact areas than NMCA. Thus, the difference between theoretically and experimentally obtained values for the ratio E/E_0 appears to result from the inter-particle adiabatic bonding of GDS.

Results and discussion

Structure parameters

The case of strengthening in particle-reinforced metal matrix composites has been extensively studied in the past. Many dislocation models have been designed to account for strengthening in this class of materials. However, most of these models tend to underestimate the strengthening increment in the metallic matrix due to the presence of reinforcement particles. Some researchers [10] believe that this underestimation is due to the neglect of another, very different contribution to composite strengthening, namely load-sharing. Unlike precipitation or dispersion hardened alloys, the volume fraction of the reinforcing phase in GDS composites is relatively high. Also, inter-particle bonding areas fail to create a continuous network, as compared with regular MMC produced by infiltrating. In this case, the matrix sheds load to the reinforcement during straining. This concept of "load-sharing" is central to composite continuum mechanics, which predicts strengthening in particle-reinforced composites based on knowledge of the bulk metal matrix properties, the volume fraction, aspect ratio, and spatial arrangement of the particles. Since the MCA model considers the actual geometric distribution of the particles, the concept of load-sharing is inherent within it.

As-deposited composite microstructures feature a near-homogeneous distribution of particles in an aluminium matrix with low porosity (Fig. 7). Ni-based composites have a higher porosity, diminishing the mechanical properties (Fig. 8). The basic microstructural features of the Al- and Ni-based GDS composites are summarized in Table 1. In all these composites, the reinforcement inter-particle distance varies in the range of 10–200 μm, and is comparable with the soft matrix particle size (about 45 μm). Thus, the inter-particle boundaries seem to exert a similar influence on dislocation creation and motion in the matrix, as compared with the reinforcement particles.

Elastic modulus and microstructure of LPGDS composites

The microstructures of Al and Al–10%Al_2O_3 GDS coatings (shown in Figs. 1 and 2) reveal that the porosity of the Al

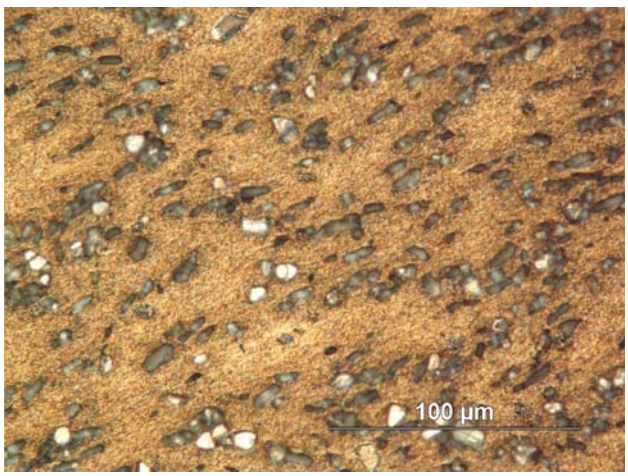

Fig. 7 Microstructure of as-deposited GDS Al–15%Al_2O_3 composite

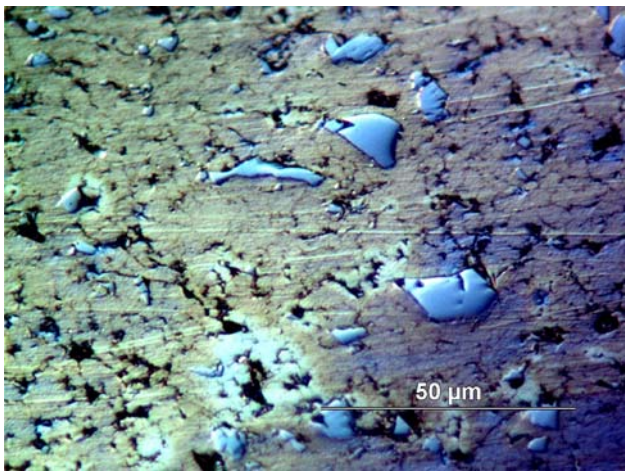

Fig. 8 Microstructure of as-deposited GDS Ni–30%TiC composite

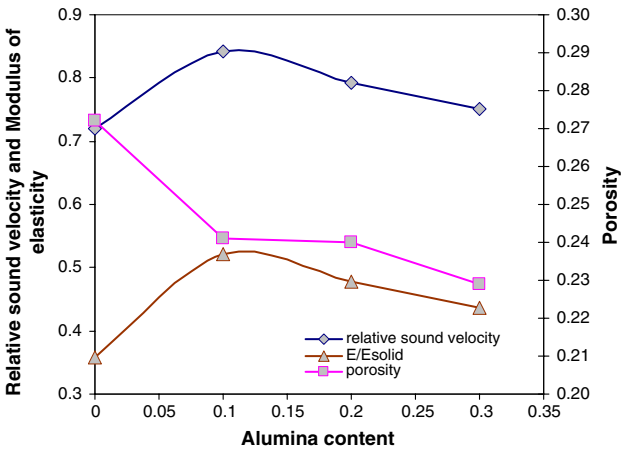

Fig. 9 Relative sound velocity, Modulus of elasticity and porosity dependences on alumina content in Al/Al_2O_3 coating composites

coating is significantly larger than that of $Al–10\%Al_2O_3$. Also, an indication of severe plastic deformation of particles may be clearly seen. It is possible to approximate the degree of inter-particle contact through their evaluation using an optical microscope. The inter-particle boundaries with adiabatic bonds are believed to be more stable for etching than those with only adhesion (Figs. 1 and 2). The thin grain boundaries within the Al particles may be seen in Fig. 1. It seems to be reasonable that inter-particle boundaries of the same thickness (for example those shown by arrows A) reveal adiabatic bonding, while thicker ones reveal only adhesion bonding (shown by arrows B). Unfortunately, a quantitative evaluation of the real adiabatic joining area is not possible through metallographic procedures. Neither is the analysis of the fracture topography useful for evaluation bonding, even in spite of the fact that areas of adiabatic bonding are clearly seen on the SEM images (Fig. 3, shown by arrows).

A quantitative analysis of the adiabatic bonding may be made by comparing the experimental and theoretical data of NMCA based on model (6). The results of the sound velocity measurement are shown in Fig. 9. The two main factors that influence sound velocity of the material are density and composition. Also, the densification process during spraying powder depends on the composition of the powder mixture. An increase in the Al_2O_3 content results in a decrease in the porosity from 0.272 to 0.229; this is due to an intensified plastic deformation of the soft Al particles. This effect is significant only for relatively small contents of Al_2O_3 (up to 10–15%). Further, increases in the content of Al_2O_3 beyond 25–30% result in an increase in porosity due to the considerable change that takes place with respect to inter-particle friction. Al_2O_3 in the shock compaction of a powder layer can significantly affect sound velocity and elasticity modulus parameters (Fig. 9). This is due to (i) a decrease in porosity, and (ii) severe local deformation of the soft Al particles in the vicinity of inter-particle contact (Fig. 3, shown by arrows).

The obtained data reveal a change in the mechanism of bond formation at porosities of about 0.2–0.25 (Fig. 10). The values of real NMCA are quite near to those obtained by sintering at high porosities. This means that severe deformation at inter-particle contact results in real adiabatic bonding of particles along the entire contact surface. It is for this reason that the NMCA parameter (Eq. 5) is measured to be quite near theoretical values calculated in accordance with the Mizusaki model (Fig. 10). The GDS shock consolidation of the powder layer up to higher density results in an increase in the contact area. However, adiabatic bonding is not achieved at all points. For this reason, the values of NMCA do not vary considerably (Fig. 11, approximation of experimental data). A simple explanation of this effect is based on the adiabatic shear

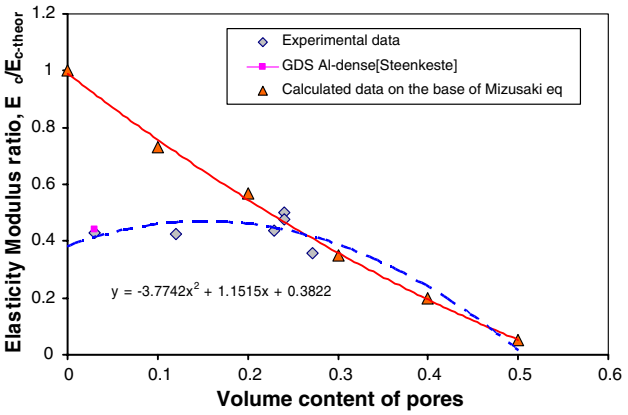

Fig. 10 Comparison of theoretical and experimental results for relative elastic modulus

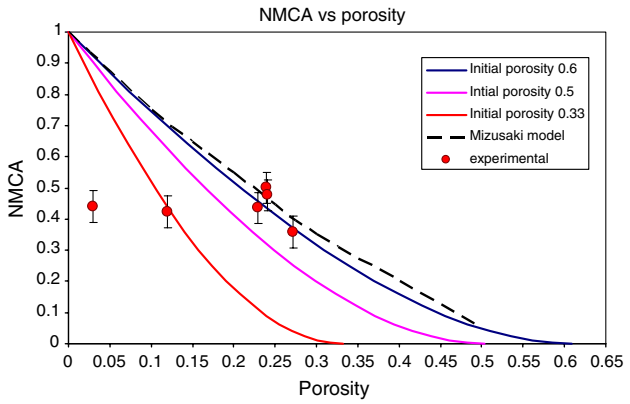

Fig. 11 NMCA model with various initial porosities as a function of porosity

band (ASB) formation process during GDS shock wave consolidation. In the case of porous powder layer formation, the inter-particle contact area is much smaller than for one of high density. The contact stresses, strains and strain rates are known to be much higher in this case and as such, ASB formation seems to be a highly probable event. When the contact area increases the stresses and strains should decrease. For smaller values of stress and strain, ASB formation is not enough, and the formation of the adiabatic bonds is not achieved. In fact, for porosities in the range of 0.03–0.23, the NMCA is about 0.4–0.42 for Al–Al_2O_3 coatings (Fig. 10). The main characteristic of GDS shock consolidation for small densities ($\theta = 0.25$–0.5) is the localization of deformation, resulting in high values of NMCA.

A validation of this model is shown in Fig. 11. One can see that the suggested shock consolidation model corresponds to experimental data in the range of $\theta = 0.25$–0.5 when the coefficients m and n of approximation (Eq. 5) fit initial porosity $\theta_o = 0.6$. A calculation of NMCA has been made using both the shock consolidation model described above and the Mizusaki model. This calculation yields similar results for $\theta_o = 0.6$, however, the curves for $\theta_o = 0.25$–0.5 differ considerably. One can assume that this behaviour is the result of localization effects at higher porosities—indeed, in the last case of higher initial porosity the number of inter-particle contacts is reduced. That leads to an increase in the contact loads and strain rates at the interface between particles.

The numerical modelling results for the impact of Al particles (diameter of particle = 60 μm) reveal that the radial velocities are higher than critical velocities only in a small region near the interface [20]. Thus, real adiabatic bonding may only be achieved in this area in spite of achieving a tight contact that may be transparent for ultrasound waves. For this reason the NMCA value does not completely characterise the area of adiabatic bonding.

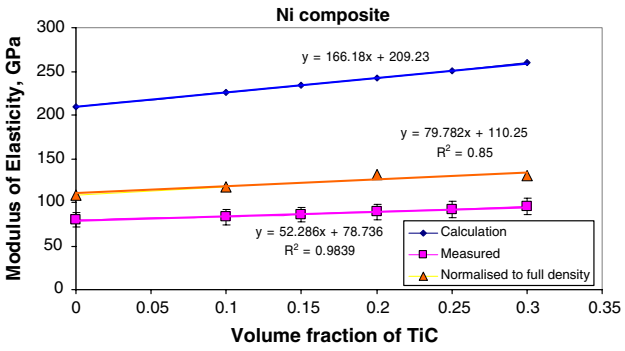

Fig. 12 Elastic modulus of Ni composite

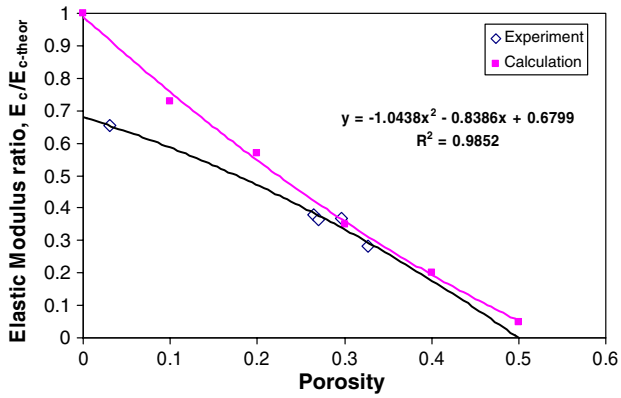

Fig. 13 Elastic modulus ratio of Ni composite

A similar behaviour in the NMCA function may be observed for Ni–TiC composites (Figs. 12 and 13). Experimental results show that the real modulus of elasticity for LPGDS Al–Al_2O_3 and Ni–TiC composite coatings is only about 40–67% that of the solid material. This suggests that the powder layer shock densification due to LPGDS gives rise to MCAs similar to that of HPGDS [21].

Conclusion

The low-pressure cold spray bonding process was described by a MCA model. By applying this model a comparison between theoretical and experimental values for the elastic modulus was possible. These values were in good agreement for higher porosity while for lower porosity the lack of full ASB formation reduced the experimental values. This model could prove quite useful for the determination of physical properties such as elasticity for the GDS process, since it relates velocity measurements directly to MCA. This is valuable since the MCA describes the real contact area of the samples. By

comparing the theoretical and experimental values of elastic modulus it would than be possible to determine the ratio of bonded area to contact area.

References

1. Alkimov AP, Kosarev VE, Papyrin AN (1990) Dokl Akad Nauk SSSR 318:1062
2. Borchers C, Gartner F, Stoltenhoff, Kreye H (2003) J Appl Phys 12 93(2):10064
3. Borchers C, Gartner F, Stoltenhoff T, Kreye H (2005) Acta Mater 53:2991. doi:10.1016/j.actamat.2005.02.048
4. Meyers MA, Benson DJ, Olevsky EA (1999) Acta mater 47(7):2089
5. Prummer R (1987) Explosivverdichting Pulvriger Substanzen Grundlagen Verfahrenergebnisse (Springer, Berlin), in German
6. Maev GrR, Leshchinsky Ev (2006) In: International thermal spray conference proceedings, Seattle, USA, 2006, CD Proceeding
7. Contreras A, Albiter A, Bedolla E, Perez R (2004) Adv Eng Mater 6(9):767
8. CenterLine (Windsor) Limited, http://www.cntrline.com, as on 07 June 2007
9. Tanga F, Meeks H, Spowart JE, Gnaeupel-Herold T, Prask H, Anderson IE (2004) Mater Sci Eng A 386:194
10. Kouzeli M, Mortensen A (2002) Acta Mater 50:39. doi:10.1016/S1359-6454(01)00327-5
11. Orrhede M, Tolani R, Salama K (1996) Res Nondestr Eval 8:23
12. Peng HX, Fan Z, Evans JRG (2001) Mater Sci Eng A 303:37. doi:10.1016/S0921-5093(00)01879-7
13. Green DJ (1998) In: An introduction to the mechanical properties of ceramics. Cambridge University Press, 336 pp
14. Mackenzie JK (1950) Proc Phys Soc Lond B63:2–11
15. Mizusaki J, Tsuchiya S, Waragai K, Tagawa H, Arai Yo, Kuwayama Y (1996) J Am Ceram Soc 79(1):109
16. Maeva E, Aczel A, Leshchinsky Ev (2006) Adiabatic shear band formation in the gas dynamic spray process. J Mater Charact (submitted)
17. Mukhopadhyay AK, Phani KK (1998) J Mater Sci 33:69. doi:10.1023/A:1004385327370
18. Mukhopadhyay AK, Phani KK (2000) J Am Ceram Soc 20:29. doi:10.1016/S0955-2219(99)00092-8
19. Martin LP, Rosin M (1997) J Am Ceram Soc 80:839
20. Papyrin AN, Kosarev VF, Klinkov SV, Alkhimov AP (2002) In: Proceedings of the international thermal spray conference, Dusseldorf, Germany, pp 380–386
21. Van Steenkiste TH, Smith JR, Teets RE (2002) Surf Coat Technol 154:237. doi:10.1016/S0257-8972(02)00018-X